ISA Transactions xxx (xxxx) xxx

Contents lists available at ScienceDirect

ISA Transactions

journal homepage: www.elsevier.com/locate/isatrans

Research article

Trajectory tracking control with state restricted gains for a magnetic pendulum using electromagnetic actuators

Rafael Perez-San Lázaro [a], Rita Fuentes-Aguilar [b], Isaac Chairez [b,*]

[a] Escuela de Ingenieria y Ciencias, Tecnologico de Monterrey Campus Guadalajara, Jalisco, Mexico
[b] Institute of Advanced Materials for Sustainable Manufacturing, Tecnologico de Monterrey Campus Guadalajara, Jalisco, Mexico

ARTICLE INFO

Article history:
Received 27 June 2022
Received in revised form 27 January 2023
Accepted 24 March 2023
Available online xxxx

Keywords:
Electromagnetic actuators
Simple pendulum
Magnetic actuation
Barrier Lyapunov function

ABSTRACT

Electromagnetic actuation results suitable for wireless driven motion, where the estimation of the force between magnetic elements is usually required. This force can lead to states where the magnetic-mechanical system remains fixed, requiring constraints to avoid the transgression of these states, and Barrier Lyapunov Functions (BLF) are useful for this purpose. This work presents an adaptive controller with BLF in a magnetic pendulum with state restrictions. It employs fixed electromagnets to induce motion on a pendulum with a permanent magnet as its bob. The force between the magnetic elements is obtained through approximation functions. A new implementation strategy for the control gains introduces the effect of state restrictions on the control action based on a control BLF. Results are analyzed in both simulations and experimental stages, which prove the advantages of employing BLF controllers in mechanical systems that require the avoidance of specific boundaries.

1. Introduction

The simple pendulum is a well-known mechanism, which consists of an element, called bob, attached to the edge of a link and with rotatory motion at its other edge. There have been several studies that analyze the dynamics of the simple pendulum [1–3]. Complementary, there are different works that present variations of this mechanism. Some of them introduce electromagnetic devices to generate motion in the pendulum, such as in [4], where they generate motion in a pendulum with an attached permanent magnet by transferring energy from a near moving conductor. Another approach is the implementation of electric passive circuits connected to coils, so that when current passes through them, a movement in the pendulum is produced [5–7]. It is also possible to include a symmetric configuration, such as the one presented in [8], which resembles the structure presented in this work, consisting in a pair of electromagnets pointing towards a central element. This particular configuration allows to have a balanced system that does not rely on a sole element to exert the motion in the pendulum.

Electromagnetic strategies embedded with mechanical systems yield several benefits, such as the fact that motion can be generated through untethered contact, making it suitable for tasks that do not require strings, allowing the reduction of the size of the devices [9]. Moreover, energy is transferred by electromagnetic waves, which, differently from other types of energy (such as X-rays), are not ionizing energy, representing no risk for people's health [10]., increasing the number of potential applications. These characteristics promote the development of novel approaches that propose innovative alternatives for issues in varied fields, especially those regarding the inclusion of living beings or that require untethered motion. Complementary, by employing electromagnetic actuators, magnetic bodies can be controlled by an external magnetic field, which can deform the composite in terms of torque, deformation, elongation, contraction or bending [11]. Additionally, these types of structures can yield some advantages, including high power efficiency, low driving voltages and fast response times [12].

Regarding the implementation of electromagnetic strategies to actuate mechanical systems, it is possible to state that it is still under development, requiring further research with respect to modeling and control [13]. For instance, the interaction that is generated between the magnetic fields and the environment increase the complexity of the modeling process. On the other hand, the non-linear properties that result from the modeling of the aforementioned interaction impacts directly on the controllability issues for these types of systems.. Furthermore, when introducing magnetic elements, it is important to avoid close contact between them, as this is the point where the force is greater [14], which can lead to undesired effects. As a consequence, controlled motion of magnetic-mechanical mechanisms must consider the mathematical model that describes the relationship between the magnetic fields and a control algorithm that can cope with the task of exerting precise movements, while avoiding a set of specific boundaries.

* Corresponding author.
E-mail address: isaac.chairez@tec.mx (I. Chairez).

https://doi.org/10.1016/j.isatra.2023.03.036
0019-0578/

For mechanical systems, boundaries are usually associated to the possibility of collision and consequent deformation for some materials [15], and in other cases, such as the one presented in this work, they can lead to physical stoppages. As a consequence, the issue of avoiding them is of particular interest for practical applications. To solve this, several control approaches have been proposed, which usually lead to optimization problems with defined constraints [16], classified as optimal control. An example of this approach is model predictive control, where the aim is to model the to-be-controlled process by solving an optimization problem [17]. Another example is extremum seeking control, where the goal is to estimate the unknown parameters of a function by optimizing it [18]. Nonetheless, different drawbacks are associated to these approaches, such as the higher computational time that results from the iterative nature of the algorithm. The introduction of Barrier Lyapunov Functions (BLF) serves to cope with the aforementioned disadvantages that result from optimal control strategies, as one of its principal characteristics is that the function tends to infinity as its state variables approach to their respective constraints, and hence assuring that the states will remain bounded [19], and its main procedure consists in defining the BLF based on the constraints that have to be considered for the system [20,21], where the algorithm may vary according with the constraints and the way in which these are defined [22].

The main contributions of this study are the design and implementation of a controller based on a BLF that contemplates state restrictions to avoid the close contact between a permanent magnet and an electromagnet; and the implementation of a self-developed testing platform that holds two electromagnets pointing towards a pendulum located at the center of the structure. Also, this pendulum has a permanent magnet as its bob, so that the magnetic fields generated by the electromagnets can interact with the one generated by the permanent magnet in the pendulum.

The document is organized as follows: Section 2 presents the problem statement of the work, where the mathematical description of the problem is introduced, along with its state variable representation and the proposal for the BLF. Fig. 4 shows the results obtained from evaluating the proposed controller in a numerical simulation environment, comparing the performance of a PID controller and the proposed BLF controller. Section 4 shows the results from the physical implementation and the description of the testing device that was used for experimental evaluation. Section 5 presents the conclusions of the work, and Appendix shows the derivative of the candidate Lyapunov function, which proves that the system is asymptotically stable and the corresponding conditions for it to remain stable.

2. Problem statement

Fig. 1 illustrates the location of the simple pendulum with respect to each electromagnet (EM), from where the symmetry of the system is appreciated. It is important to recall that the geometry of magnetic elements plays a fundamental role in the definition of the force that results from their interaction, as stated in [23]. The pendulum is composed by a rigid link l [m] and a spherical permanent magnet (PM), with mass m [kg], as its bob, and it forms an angle θ [deg] with respect to the vertical plane. Notice that after defining y_T and x_T, the rest of unknown variables can be obtained from the value of θ through trigonometric relationships.

According to the Lagrangian mechanics [24], the dynamics of the simple pendulum can be defined by:

$$ml^2\frac{d^2}{dt^2}\theta + mglsin(\theta) = \tau \tag{1}$$

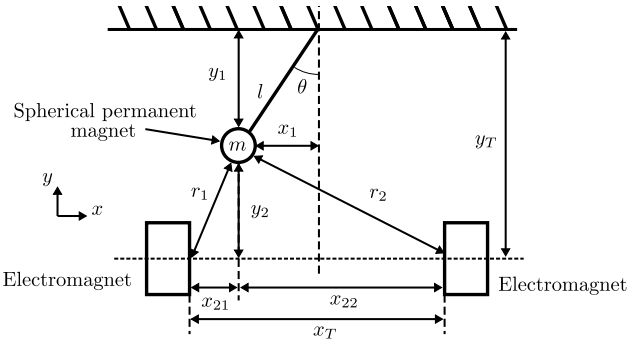

Fig. 1. Simple pendulum diagram.

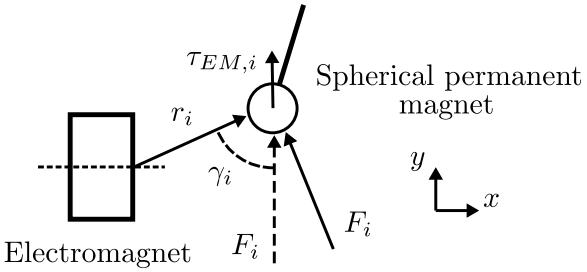

Fig. 2. Torque generated by each electromagnet.

where τ [Nm] is the resulting torque generated by the combined action of both EMs. Therefore:

$$\tau = \sum_{i=1}^{2} \tau_{EM,i} \tag{2}$$

where $\tau_{EM,1}$ and $\tau_{EM,2}$ describe the torque generated by each EM. For each case, the torque can be defined as:

$$\tau_{EM,i} = r_i \times F_i \tag{3}$$

where r_i [m] with $i = 1, 2$ is the distance between each EM and the PM, as defined in the diagram from Fig. 1, whereas F_i [N] with $i = 1, 2$ is the force that each EM must exert to generate a torque in the bob of the pendulum. This can be appreciated in Fig. 2.

Equivalently, (3) can be expressed considering the angle γ_i [deg], which is formed between r_i and F_i, yielding

$$\tau_{EM,i} = r_i \cdot F_i \cdot sin(\gamma_i) \tag{4}$$

Notice that the solid arrow depicting F_i corresponds to the component force vector that has a greater effect on the resulting torque. Nonetheless, for this case, θ holds small variations and hence, it is possible to consider only the force component represented with the dotted arrow as a suitable approximation for F_i. According to the coordinate system presented in both Figs. 1 and 2, to define the torque generated by each EM, only the y component of the force F_i is required.

The aforementioned component of the force may be computed using different methodologies [25–27], where most of them lead to complex equations. This paper considers the utilization of the approximation function along with the values of its parameters as presented in [28], to define the required component of the force and consequent torque generated by the EM on the PM, so that dynamics in (1) can be fully defined.

To compute the y-component of the force exerted in the PM by each EM, the following expressions are utilized:

$$F_y = \left[\frac{\left(\frac{L_S}{2}\right)^4}{\left(\frac{L_S}{2}\right)^4 + \left(y - \frac{L_L}{2}\right)^4} - \frac{\left(\frac{L_S}{2}\right)^4}{\left(\frac{L_S}{2}\right)^4 + \left(y + \frac{L_L}{2}\right)^4} \right] F_{y,m} \tag{5a}$$

$$F_{y,m} = \frac{1}{k - 0.244\, exp\left[-2\left(\frac{L_L}{L_S} - 1\right)\right]} \frac{F_0}{L_S} \frac{d_e^2}{x + d_e} \tag{5b}$$

where the parameters L_S [mm], L_L [mm], and k relate to the geometry of the magnetic elements, whereas F_0 [N] and d_e [mm] describe the interaction between the magnetic forces, and they result from an experimental characterization procedure between the EM and the PM. Nonetheless, the effect that the current that passes through the EMs has on the resulting force is not yet considered, defined by the following equation:

$$mmF = N * i \tag{6}$$

which describes the magnetomotive force mmF $[At]$ in an EM [29], where N $[t]$ is the number of turns and i $[A]$ is the current that passes through the EM. Based on this relationship, it is possible to state that the current generates a linear effect on the force that it produces, and hence, the parameters that describe the interaction between magnetic forces can be redefined as linear functions that depend on the current i, yielding:

$$F_0(i) = m_{F_0} i + b_{F_0} \tag{7a}$$

$$d_e(i) = m_{d_e} i + b_{d_e} \tag{7b}$$

where for both cases, the function is characterized by the slope m and the y-intercept b. Notice that each one of the two EMs has its own approximation function, with two different currents passing through each EM, making it necessary to consider two currents i_1 and i_2. Then, (4) can be restated as:

$$\tau_{EM,i} = r_i \cdot F_{y,i} \cdot sin(\gamma_i) \tag{8}$$

Moreover, for the proposed scenario, the angle θ is defined only by the effect of one EM at a time, that is, there is no time when both EMs are active simultaneously, and therefore, it is necessary to include an activation function within the definition of the force $F_{y,i}$, which can be defined as:

$$\xi(\theta^*) = \begin{cases} 1 & \text{for} \quad \theta^* > 0 \\ 0 & \text{for} \quad \theta^* \leq 0 \end{cases} \tag{9}$$

included within the control design

2.1. State variable representation

Let consider the definition of state variables

$$x_1 = \theta \tag{10a}$$

$$x_2 = \dot{\theta} \tag{10b}$$

so that the dynamic model in (1) can be stated as

$$\dot{x}_1 = x_2 \tag{11a}$$

$$\dot{x}_2 = (ml^2)^{-1} (\tau - mlgsin(x_1)) \tag{11b}$$

which, after considering (2) and (4), it results

$$\dot{x}_1 = x_2 \tag{12a}$$

$$\dot{x}_2 = (ml^2)^{-1} \left(r_1 \cdot F_1 \cdot sin(\gamma_1) + r_2 \cdot F_2 \cdot sin(\gamma_2) - mlgsin(x_1) \right) \tag{12b}$$

From here, the expressions for F_1 and F_2 are already defined and depend only on the current i_1 and i_2, respectively.

The control problem consists in designing the currents i_1 and i_2, such that the tracking error can be stabilized asymptotically. The tracking error δ_1 is defined as

$$\delta_1 = \theta^* - \theta \tag{13}$$

where θ^* is the proposed reference trajectory and it satisfies:

$$\ddot{\theta}^* = h \tag{14}$$

where h a continuous scalar function with bounded derivative

$$\left|\dot{h}\right| \leq dh+, \quad dh+ > 0 \tag{15}$$

2.2. Barrier Lyapunov function

Introducing the following variables $x_1^* = \theta^*$ and $x_2^* = \dot{\theta}^*$, the dynamics of the tracking error $\delta_1 = x_1^* - x_1$ is described by:

$$\dot{\delta}_1 = \delta_2 \tag{16a}$$

$$\dot{\delta}_2 = h - \left(ml^2\right)^{-1} (r_1 \cdot F_1 \cdot sin(\gamma_1) + r_2 \cdot F_2 \cdot sin(\gamma_2) - mglsin\,(x_1)) \tag{16b}$$

The design of the control action is based on the stages corresponding to the traditional backstepping procedure. The first stage forces δ_2 to track an auxiliary desired reference trajectory, which corresponds to $\delta_2^* = -\lambda_1 \delta_1$, with $\lambda_1 > 0$. The second stage of the control design considers that F_i, for $i = 1, 2$, must be designed to force that $e_2 = \delta_2 - \delta_2^*$ converges to the origin faster than the equivalent differential equation of δ_1.

According to the statement for the first stage of the control design, the equivalent auxiliary dynamics for the deviation $e_1 = \delta_1 - \delta_1^*$ yield

$$\dot{e}_1 = \delta_2 + \lambda_1 \delta_1 \tag{17}$$

For the second stage, the deviation e_2 must be driven to the origin considering the following dynamics

$$\dot{e}_2 = \dot{\delta}_2 - \dot{\delta}_2^* \tag{18}$$

Using the dynamics of δ_2 and the expression of δ_2^*, the following expression holds:

$$\dot{e}_2 = h - \left(ml^2\right)^{-1} (r_1 \cdot F_1 \cdot sin(\gamma_1) + r_2 \cdot F_2 \cdot sin(\gamma_2) - mglsin\,(x_1)) - \lambda_1 \delta_2 \tag{19}$$

As it was previously mentioned, the function ξ decides which of the two EMs is preferred to solve the stabilization of e_2. For instance, with the same input current and considering the operational limits of the EMs, if $\xi > 0$, then F_2 is larger than F_1 and hence, the stabilization problem can be solved.

Based on the design conditions for the controllers F_1 and F_2, and considering (9), a feasible approach to state them could be

$$F_1 = r_1^{-1} sin^{-1}(\gamma_1) \left[\left(ml^2 h + mglsin\,(x_1)\right) \xi(x_1^*) + ml^2 \left(v_1 - \lambda_1 \delta_2\right) \xi(x_1^*) \right] \tag{20}$$

$$F_2 = r_2^{-1} sin^{-1}(\gamma_2) \left[\left(ml^2 h + mglsin\,(x_1)\right) (1 - \xi(x_1^*)) + ml^2 \left(v_2 - \lambda_1 \delta_2\right) (1 - \xi(x_1^*)) \right] \tag{21}$$

Notice that when $\xi = 0$, F_2 is active, whereas when $\xi = 1$, F_1 is active. Furthermore, the selected combination of forces F_1 and F_2 allows to have a continuous evolution when $x_1^* = 0$. Then, the design process of v_i for $i = 1, 2$ must take into account the following conditions:

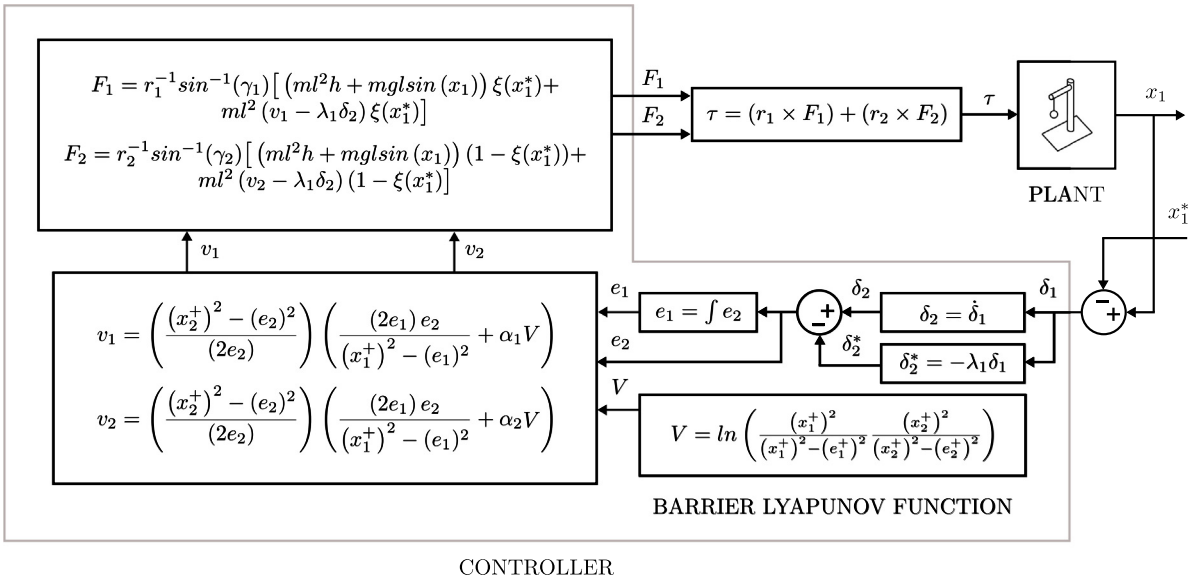

Fig. 3. Diagram of the control scheme.

- The angle x_1 is bounded ($x_1^- \leq x_1 \leq x_1^+$), as well as its derivative ($x_2^- \leq x_2 \leq x_2^+$).
- All the parameters in the simple magnetic pendulum are known.
- The actual current modifying the actuator behavior is the averaged value over a period of time T_c.

Then, the variable e_1 is governed by the following differential equations:

$$\dot{e}_1 = e_2 \tag{22a}$$

$$\dot{e}_2 = h - \left(ml^2\right)^{-1}\left(r_1 \cdot F_1 \cdot sin(\gamma_1) + r_2 \cdot F_2 \cdot sin(\gamma_2) - mglsin\left(x_1\right)\right) - \lambda_1\delta_2 \tag{22b}$$

The proposed controller

$$\tau = \sum_{i=1}^{2} r_i \cdot F_{EM,i} \cdot sin(\gamma_i) \tag{23}$$

includes a degree of freedom in both F_1 and F_2, denoted as v_1 and v_2, respectively, which are defined after realizing the corresponding Lyapunov stability analysis. The candidate BLF can be defined as:

$$V = ln\left[\frac{\left(x_1^+\right)^2}{\left(x_1^+\right)^2 - (e_1)^2} \cdot \frac{\left(x_2^+\right)^2}{\left(x_2^+\right)^2 - (e_2)^2}\right] \tag{24}$$

where the inclusion of coordinate bounds is considered. Notice the symmetry of the bounds contained in the BLF. According to the stability analysis of Lyapunov, in order to make (24) asymptotically stable, it has to fulfill the following conditions:

1. The proposed function is positive definite
2. If e_1 and e_2 are both zero, then $V = 0$
3. If e_1 and e_2 tend to infinity, then V tends to infinity
4. The time derivative of V is negative definite

The first 3 properties are clearly fulfilled, whereas property 4 is proven in Appendix

Based on the 4 previous conditions. The definitions of force F_1 and F_2 that make the system stable are defined by:

$$v_1 = \left[\frac{\left(x_2^+\right)^2 - (e_2)^2}{(2e_2)}\right]\left[\frac{(2e_1)\,e_2}{\left(x_1^+\right)^2 - (e_1)^2} + \alpha_1 V\right] \tag{25}$$

with $\alpha_1 > 0$ in (20), and

$$v_2 = \left[\frac{\left(x_2^+\right)^2 - (e_2)^2}{(2e_2)}\right]\left[\frac{(2e_1)\,e_2}{\left(x_1^+\right)^2 - (e_1)^2} + \alpha_2 V\right] \tag{26}$$

with $\alpha_2 > 0$ in (21).

From (25) and (26), it may seem that there could be a problem with the zero at the denominator. However, this is not an issue as Zubov's theorem justifies its implementation [30].

Remark 1. The implementation of the BLF itself does not justify the operation within a safety region. Instead, the controller does it based on the gains, which at the same time are defined by the BLF. For instance, if the current is too big when approaching the bounds, then the adaptive gains guarantee the operation within the safety region.

Fig. 3 shows the control scheme that is implemented in this work. Notice how the backstepping approach is evident in the diagram. However, the Barrier Lyapunov Function is introduced within the definition of τ, where e_1 and e_2 are used as stated in (25) and (26).

3. Numerical results

The results obtained from the numerical simulation allows to compare the two proposed strategies. The comparison is made between a PID controller, where no state restrictions are included in the control design, and the control based on a BLF that includes the restrictions. This comparison is made to illustrate the properties of BLF algorithms over traditional controllers, such as PID. The simulated system considers the following parameters: $m = 0.1$ kg, $xT = 0.18$ m, $yT = 0.085$ m, $g = 9.81$ m/s^2, $l = 0.082$ m, whereas for the case of the BLF controller: $\lambda = \pi/4$, $x_1^+ = 2.4$, $x_2^+ = 2.8$, $\alpha_1 = \alpha_2 = 450$, and for the PID: the proportional gain $k_p = 500$, the derivative gain $k_d = 300$, and the integral gain $k_i = 10$.

At first, an arbitrary sine wave is proposed to serve as reference for the system so that its performance can be evaluated. Nevertheless, a different trajectory can be followed as long as it exists within the boundaries of the pendulum. Fig. 4 shows the trajectory tracking for the system with restrictions and without restrictions. Notice that both controllers can cope with the trajectory tracking task, yielding a similar performance.

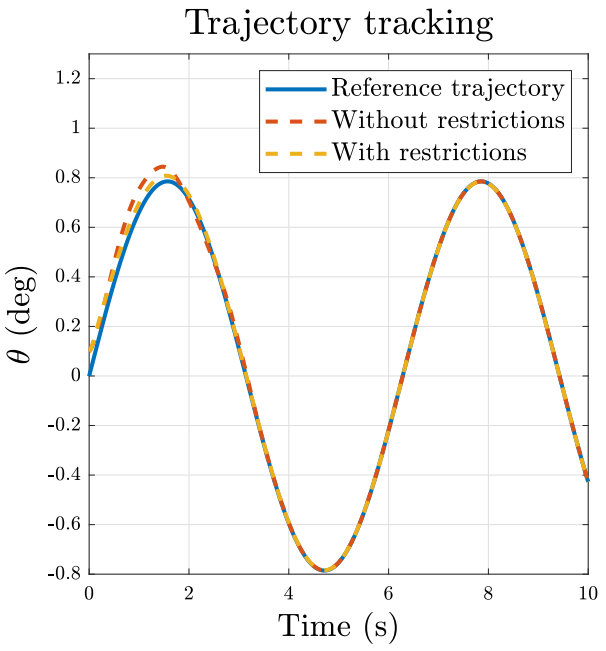

Fig. 4. Trajectory tracking.

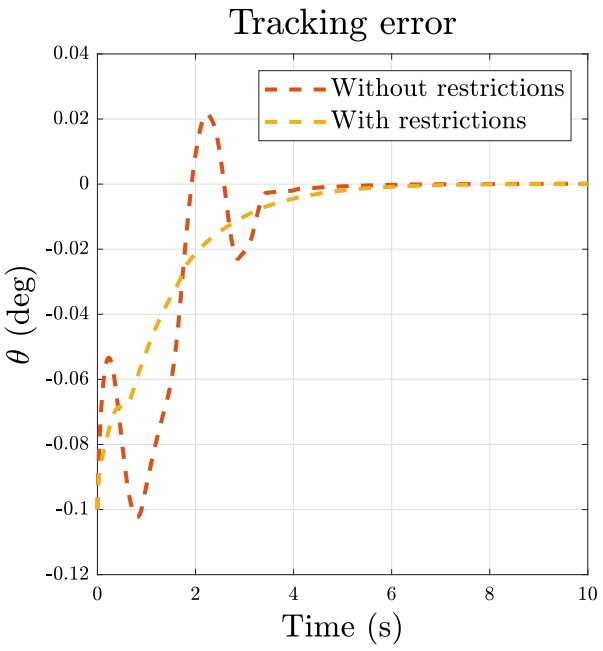

Fig. 5. Trajectory tracking error.

The advantage that the BLF controller has over the PID controller becomes evident when the tracking error from Fig. 5 is analyzed, where it is possible to observe that the tracking error varies within a specific range. Such a fact is established from the definition of the constraints for the restricted approach. On the contrary, when no boundaries are contemplated, the specified constraints of the tracking error are transgressed. This is particularly undesired for the magnetic pendulum system as it can reach a state where the PM is at a defined distance from the EM so that the magnetic force between these elements is enough to set the pendulum fixed in a specific position, making it impossible to move by itself. Hence, for this case, it is necessary to guarantee that the pendulum will not reach those limits. From here, the main advantage from the implementation of the BLF controller becomes evident for systems where the avoidance of certain boundaries results of paramount importance. Moreover, from Fig. 5, it is possible to observe that the tracking error converges to zero independently from the inclusion of restrictions, and almost at the same time.

As it was previously mentioned, a switching scheme is proposed for the magnetic pendulum, where the switching action alternates the activation of the two EMs. Fig. 6 describes this switching approach, where it is possible to observe that there is no case where both EMs remain active, as defined by the activation function in (9). It is important to recall that the signal of the exerted force follows a sine form as the reference signal is of the same kind. For different cases, the force could depict different behaviors.

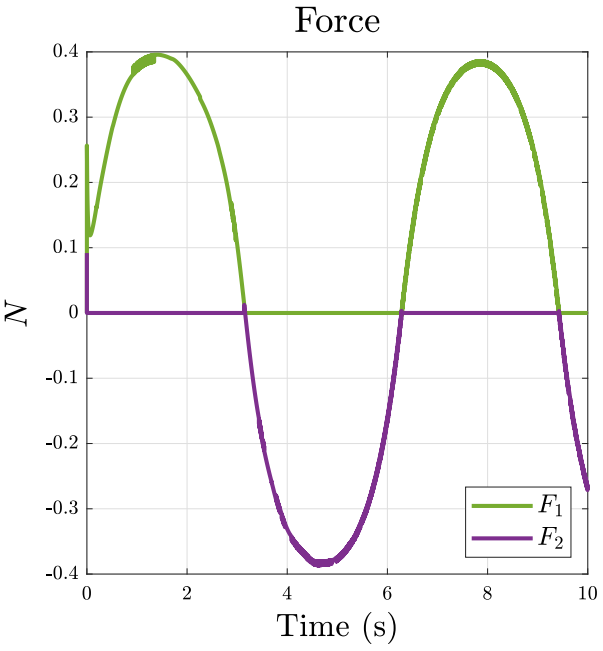

Fig. 6. Force applied by the electromagnets.

4. Experimental results

The parameters for the system are the same ones that were used for the simulation. For the BLF controller, the following tuning parameters were used: $\lambda = \pi/4, x_1^+ = 1.8, x_2^+ = 1.5, \alpha_1 = \alpha_2 = 130$. The physical implementation results consider two different cases. The first case only comprehends the effect of the activation of only one EM, avoiding the switching scheme of the complete system. This approach is generated by a trajectory that is defined exclusively by negative θ values, and therefore yielding just one case of the activation function (9). Besides, the trajectories follow triangular-like shapes to show that the algorithm is capable of following different references apart from the sine wave shown in the numerical simulations section. Notice from the reference signal that the minimum value oscillates around -8 degrees, according to the boundaries of the system, which are defined experimentally in order to avoid the PM from getting so close to the EM that the pendulum gets into a fixed position. As the system is symmetrical, then the boundary for the negative θ values is the same for positive θ values.

The first experiment is illustrated in Fig. 7, where the trajectory tracking is shown, following a triangular-like reference signal. Also, its respective tracking error is shown. Notice that

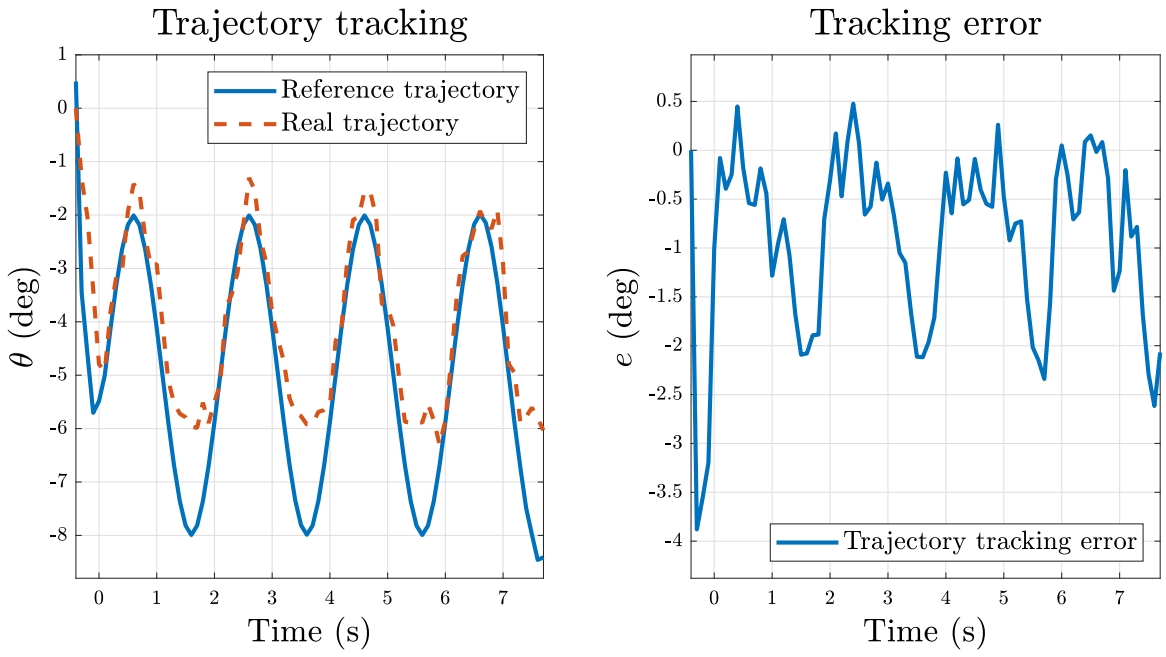

Fig. 7. Triangle-like wave controlled by one electromagnet.

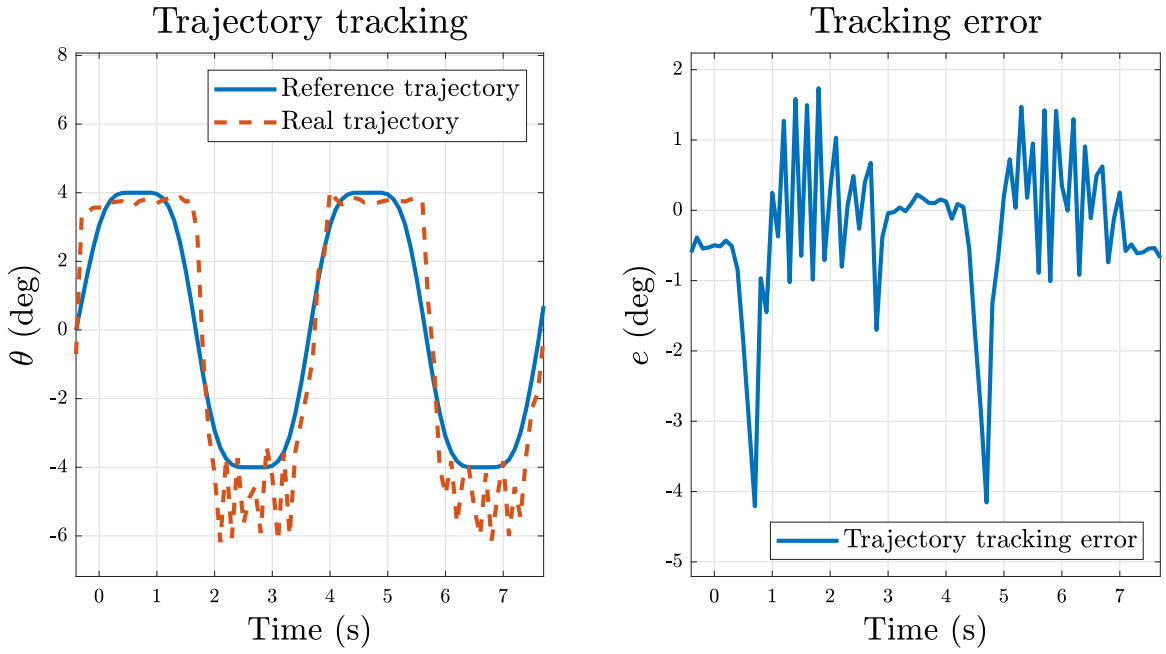

Fig. 8. Clipped sine wave controlled by two electromagnets.

the system has a degree of difficulty while trying to track the reference at the edges of the reference signal. However, this effect can still be diminished through an adjustment of the gains of the respective BLF controller. Recall that for this stage of physical implementation, the algorithm has to be discretized so that it can be embedded within the microcontroller architecture, which leads to an increase in the number of variables that affect the performance of the outcome.

For the second experiment, a clipped sine wave is defined as reference signal. Notice that for this case, both negative and positive values are considered, requiring both EMs to get activated through the proposed switching scheme. Fig. 8 illustrates the ability of the system to track the reference trajectory, along with its tracking error. It is possible to observe that the regions where the error increases have a more abrupt change. As for the first case, it is possible to reduce the tracking error generated by the system through different approaches, including the proposal of a smoother reference trajectory instead of those with abrupt changes such as the ones proposed for the two cases of the physical implementation. Regardless of the tracking error signal for both of the analyzed cases, the system presented the desired behavior as expected from the BLF controller, as there was no case when the pendulum got in a fixed position due to the proximity of the PM with the EMs as a consequence of a state that goes beyond the established boundaries. For the experimental section, only the BLF controller was implemented, as the purpose of the work is to prove that it is useful to avoid the PM from getting

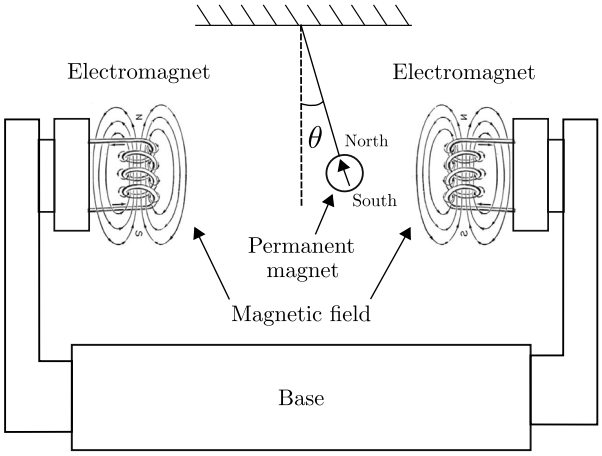

Fig. 9. Diagram of the testing device.

in close contact with the EMs, so no comparison with the PID controller is required.

4.1. Testing device

A self-developed testing device is used to evaluate the performance of the proposed BLF controller. It is a simple pendulum with its degree of freedom defined by the angle θ, as illustrated in Fig. 9, where the location of the rotation axis can be observed. From this figure, it is possible to observe the mechanical structure that is composed by the base and the supporting structures that hold the EMs. Complementary, the electronic devices associated to the operation of the EMs are immersed within the base of the structure. Recall that the PM generates a constant magnetic field with a defined direction, which is described in Fig. 9. Moreover, this structure is designed based on the diagram from Fig. 1, holding the same geometrical relationships. Regarding the dimensions of the testing device, the relevant variables are the sames as the ones described within the numerical results section, which include parameters such as the mass of the bob, the link of the pendulum, and the geometrical dimensions of the system.

The complete structure of the testing device is made from polylactic acid (PLA) including the base and the supports that hold each EM. This material allows to avoid any interference that the magnetic fields could generate from its interaction, as it is not a magnetic material. Furthermore, this material is compatible with 3D printing techniques, allowing the fabrication of pieces directly from the previously CAD designs by means of Fused Deposition Modeling techniques. Some of the properties of PLA, such as its mechanical characteristics and manufacturing easiness, yield a better implementation feasibility simplifying the required manufacturing processes [31,32], such as plastic injection, to obtain a testable device. Furthermore, PLA based techniques represent lower production costs in comparison with more traditional processes [33]. The PLA pieces are printed with a 3D printer from Creality (Ender-3 pro), which has a printing area of 220 $\times$ 220x255 mm. It can work with a variety of materials, such as PLA and ABS. The printing process is set at 60° as the hotbed temperature, and 210 °C as the nozzle temperature. The structures that were previously designed in Solidworks are then exported as Stereolithography Mesh (STL) files. Then, these files are imported within the Ultimaker Cura environment, where the printing settings are set with a Standard Quality profile, to be printed at 60 mm/s, along with 10% infill and a grid infill pattern. Finally, a g-code file is generated for the Creality printer to produce the desired structures.

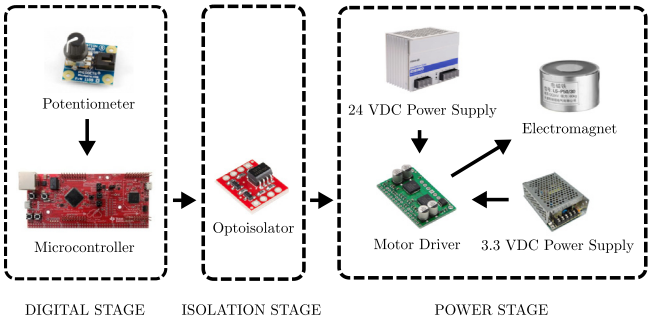

Fig. 10. Instrumentation of the testing device.

The device implements a digital and a power stage within the instrumentation, which are connected by an isolation stage that implements the Sparkfun optoisolator BOB-09118. These three stages are connected as described in Fig. 10. For the case of the digital stage, a Texas Instruments microprocessor is considered (TIVA C Series TM4C1294). This device has an ARM Cortex-M4 nucleus that works at 120 MHz, with 12-bits analog-digital converters, 256 Kb SRAM, and 1MB Flash memory. This device can execute complex algorithms without any additional processing unit, and serves to implement the control scheme along with a pulse-width modulation (PWM) signal that is used to regulate the current that is induced into the EMs (Electromagnet LS-P50/30), and its effect over the spherical PM, which has a diameter of 19.05 mm. Additionally, this stage considers a rotatory 10KΩ potentiometer (Phidgets 1109_0), which is located at the pendulum's rotation axis and measures the angle θ that is formed between the pendulum and the vertical plane. The power stage considers the inclusion of the Pololu Dual MC33926 Motor Driver Carrier, which is in charge of regulating the current that passes through the EMs. This shield allows to control two brushed DC motors and can operate from 5 to 28 VDC, while delivering a signal with up to continuous 3 A per motor (5 A peak). It is compatible with 3.3 V and 5 V systems. It also allows PWM operation of up to 20 kHz. This device has some characteristics that provide a degree of robustness and protection, including transient operation of up to 40 V, under-voltage shutdown, over-temperature shutdown, and over-current limiting via PWM. The EMs that are used in the system work at 24 V, with a maximum current of 670 mA, consuming around 8 W and generating a holding force of 60 kg. They are made from mild steel and weight around 350 g. This stage also considers the voltage sources that provide the system with the energy that it requires. The device includes a 24VDC voltage source (PSB24-480) from RHINO, which allows an amperage rating up to 20 A, and a 3.3VDC voltage source (HTS-15-3.3), which is manufactured by Haitaik and it can provide up to 3 A.

The prototype is constructed to analyze the interaction between the PM and the EMs. Notice that in Fig. 11(a) both EMs remain fixed in their respective structures (made from PLA) and that are arranged in a symmetrical array, both pointing towards the center of the structure, where the PM is located. Furthermore, the rotation axis is at the upper region of the structure, as described in Fig. 9. From here, it is also possible to observe the whole mechanical structure, which, as it was mentioned, is entirely made from PLA. The pendulum is not clearly observed in this figure as it is shown in a front view. However, the pendulum is better appreciated in Fig. 11(b), where the instrumentation of the device is also shown. Typically, the instrumentation is located inside the base of the testing device, yet, it was located outside for illustrative purposes. Additionally, the variable resistor used as angular position sensor is also better appreciated in Fig. 11(b).

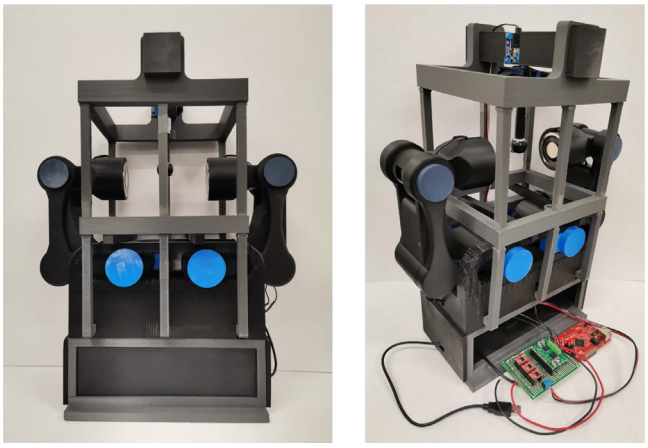

(a) Front view (b) Isometric view

Fig. 11. Testing device.

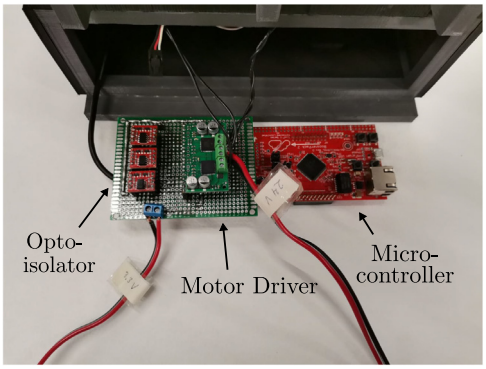

Fig. 12. Instrumentation of the testing device.

The power sources that are connected to the circuits of the device are located at the back of the testing device, but this view is omitted as it does not contribute for the purposes of this work. Nonetheless, they have to be connected for the device to work correctly. The power source supply energy to different parts of the system. For instance, the 3.3VCD is used for the digital section of the power stage, while the 24VDC is employed for the EMs activation. From the figures of the physical prototype, it is possible to observe that the prototype has a USB cable, which serves to connect the microcontroller to a computer. However, the system can be set so that the connection to the personal computer is not necessary, and leaving the system as a standalone device.

The rest of the electronic devices that are required so that the system can operate correctly are shown in Fig. 12, composed by the digital stage (microcontroller), the power stage (motor driver) and the isolation stage (optoisolator), all of them located within the PLA base of the device.

5. General discussion and conclusions

This work presents the implementation of a controller that considers state constraints, which is implemented to drive the system towards the proposed reference trajectories. A controller based on the BLF showed its capability of avoiding the system from getting close to a pair of boundaries established in the symmetrical configuration of the prototype. This property is particularly useful for mechanical systems where the avoidance of boundaries is of paramount importance, such as in arrangements that include magnetic elements that can get in close contact. This statement is justified with the results obtained from both the numerical simulation and experimental setup. Analysis regarding other properties from the controllers is not considered as relevant as the main useful advantage is related to the boundaries of the system. Furthermore, the dynamics of the system included an approximation function to define the force that each EM exerts over the PM. The accuracy of this approximation is out of the scope of this manuscript. Finally, the self-developed testing device served to analyze the proposed magnetic-mechanical mechanism, which is expected to serve as a basis for the development of more complex systems that involve untethered actuation employing electromagnets and magnetic materials.

Funding

The paper was prepared with the partial financial support of the Tecnologico de Monterrey, Institute of Advanced Materials for Sustainable Manufacturing under the grant Challenge-Based Research Funding Program 2022 number I006-IAMSM004-C4-T2-T.

Declaration of competing interest

The authors declare that they have no known competing financial interests or personal relationships that could have appeared to influence the work reported in this paper.

Appendix. Derivative of V

Considering the candidate Lyapunov function

$$V = ln\left[\frac{\left(x_1^+\right)^2}{\left(x_1^+\right)^2-(e_1)^2}\cdot\frac{\left(x_2^+\right)^2}{\left(x_2^+\right)^2-(e_2)^2}\right] \tag{A.1}$$

The full-time derivative of this function satisfies the following identity

$$\begin{aligned}\dot{V} = &\left[\frac{\left(x_1^+\right)^2}{\left(x_1^+\right)^2-(e_1)^2}\right]^{-1}\left(x_1^+\right)^2-\frac{(-2e_1)\,\dot{e}_1}{\left[\left(x_1^+\right)^2-(e_1)^2\right]^2}+\\ &\left[\frac{\left(x_2^+\right)^2}{\left(x_2^+\right)^2-(e_2)^2}\right]^{-1}\left(x_2^+\right)^2-\frac{(-2e_2)\,\dot{e}_2}{\left[\left(x_2^+\right)^2-(e_2)^2\right]^2}=\\ &\left[\frac{(2e_1)\,\dot{e}_1}{\left(x_1^+\right)^2-(e_1)^2}\right]+\left[\frac{(2e_2)\,\dot{e}_2}{\left(x_2^+\right)^2-(e_2)^2}\right]\end{aligned} \tag{A.2}$$

The simplification of Eq. (A.2) using the dynamics of the pendulum leads to

$$\begin{aligned}\dot{V} = &\left[\frac{(2e_1)\,e_2}{\left(x_1^+\right)^2-(e_1)^2}\right]+\left[\frac{(2e_2)}{\left(x_2^+\right)^2-(e_2)^2}\right]\\ &\left[h-\left(ml^2\right)^{-1}\left(r_1\cdot F_1\cdot sin(\gamma_1)+\right.\right.\\ &\left.\left.r_2\cdot F_2\cdot sin(\gamma_2)-mglsin\left(x_1\right)\right)-\lambda_1\delta_2\right]\end{aligned} \tag{A.3}$$

Considering (20) and (21), which describe the definitions for F_1 and F_2, it is necessary to analyze both cases where $\xi = 0$ and $\xi = 1$.

For the case when $\xi = 1$, the derivative of the Lyapunov function remains

$$\dot{V} = \frac{2e_1e_2}{(x_1^+)^2-(e_1)^2}-\frac{2e_2}{(x_2^+)^2-(e_2)^2}v_1 \tag{A.4}$$

And defining the degree of freedom v_1 as

$$v_1 = \left[\frac{\left(x_2^+\right)^2 - (e_2)^2}{(2e_2)}\right]\left[\frac{(2e_1)\, e_2}{\left(x_1^+\right)^2 - (e_1)^2} + \alpha_1 V\right] \tag{A.5}$$

it leads to $\dot{V} = -\alpha_1 V$. Similarly, for the other case where $\xi = 0$, the derivative of the Lyapunov function is

$$\dot{V} = \frac{2e_1 e_2}{(x_1^+)^2 - (e_1)^2} - \frac{2e_2}{(x_2^+)^2 - (e_2)^2} v_2 \tag{A.6}$$

And defining the degree of freedom v_2 as

$$v_2 = \left[\frac{\left(x_2^+\right)^2 - (e_2)^2}{(2e_2)}\right]\left[\frac{(2e_1)\, e_2}{\left(x_1^+\right)^2 - (e_1)^2} + \alpha_2 V\right] \tag{A.7}$$

it yields $\dot{V} = -\alpha_2 V$. For both cases, the derivative of the Lyapunov function is negative as long as α_1 and α_2 are positive for the differential equation of V.

References

[1] Borghi R. Simple pendulum dynamics: revisiting the Fourier-based approach to the solution. 2013, ArXiv: Classical Physics.
[2] D. Amrani MB. Approximation expressions for the large-angle period of a simple pendulum revisited. Rev Mex Fis 2007.
[3] Quiroga GD, Ospina-Henao PA. Dynamics of damped oscillations: physical pendulum. Eur J Phys 2017;38(6):065005.
[4] Boeck T, Sanjari SL, Becker T. Dynamics of a magnetic pendulum in the presence of an oscillating conducting plate. PAMM 2021;20(1).
[5] Kadjie AN, Tuwa PRN, Woafo P. An electromechanical pendulum robot arm in action: Dynamics and control. Shock Vib 2017;2017:1–13.
[6] Teh SH, Chan KH, Woo KC, Demrdash H. Rotating a pendulum with an electromechanical excitation. Int J Non-Linear Mech 2015;70:73–83.
[7] Mogo JB, Woafo P. Dynamics of a nonlinear electromechanical device with a pendulum arm. J Comput Nonlinear Dyn 2007;2(4):374–8.
[8] Giron-Sierra JM. A simple device and a project for the nonlinear control systems laboratory. IEEE Trans Educ 2001;44(2):144–50.
[9] Banerjee H, Ren H. Electromagnetically responsive soft-flexible robots and sensors for biomedical applications and impending challenges. In: Electromagnetic actuation and sensing in medical robotics. Springer Singapore; 2017, p. 43–72.
[10] Lai HC, Singh NP. Medical applications of electromagnetic fields. IOP Conf Ser: Earth Environ Sci 2010;10:012006.
[11] Do TN, Phan H, Nguyen TQ, Visell Y. Miniature soft electromagnetic actuators for robotic applications. Adv Funct Mater 2018;28(18):1800244.
[12] Cao A, Kim J, Lin L. Bi-directional electrothermal electromagnetic actuators. J Micromech Microeng 2007;17(5):975–82.
[13] Marino H, Bergeles C, Nelson BJ. Robust electromagnetic control of microrobots under force and localization uncertainties. IEEE Trans Autom Sci Eng 2014;11(1):310–6.
[14] Mohdeb N, Allag H, Hacib T. A new approximation for calculating attraction force in cylindrical permanent magnets arrays and cylindrical linear single-axis-actuator. Prog Electromagn Res C 2019;91:213–25.
[15] Eugster SR, Glocker C. Constraints in structural and rigid body mechanics: a frictional contact problem. Ann Solid Struct Mech 2013;5(1–2):1–13.
[16] Soner HM. Optimal control with state-space constraint I. SIAM J Control Optim 1986;24(3):552–61.
[17] Schwenzer M, Ay M, Bergs T, Abel D. Review on model predictive control: an engineering perspective. Int J Adv Manuf Technol 2021;117(5–6):1327–49.
[18] Dochain D, Perrier M, Guay M. Extremum seeking control and its application to process and reaction systems: A survey. Math Comput Simulation 2011;82(3):369–80.
[19] Sachan K, Padhi R. Barrier Lyapunov function based output-constrained control of nonlinear Euler-Lagrange systems. In: 2018 15th International conference on control, automation, robotics and vision. IEEE; 2018.
[20] Kemao M, Wang Q, Wang J. Controller design for systems with state constraints. In: 2016 35th Chinese control conference. IEEE; 2016.
[21] Tee KP, Ge SS, Tay EH. Barrier Lyapunov functions for the control of output-constrained nonlinear systems. Automatica 2009;45(4):918–27.
[22] Ames AD, Coogan S, Egerstedt M, Notomista G, Sreenath K, Tabuada P. Control barrier functions: Theory and applications. In: 2019 18th European control conference. 2019, p. 3420–31.
[23] Camacho V. Alternative method to calculate the magnetic field of permanent magnets with azimuthal symmetry. Rev Mex Fis 2013.
[24] Morin D. Introduction to classical mechanics. Cambridge, England: Cambridge University Press; 2012.
[25] Furlani E. Permanent magnet and electromechanical devices : materials, analysis, and applications. San Diego, Calif. London: Academic; 2001.
[26] Jebelli A, Mahabadi A, Yagoub MCE, Chaoui H. Magnetic force calculation between magnets and coils. Int J Phys 2020;8(2):71–80.
[27] Kwon M, Jung J, Jang T, Sohn S. Magnetic forces between a magnet and a solenoid. Phys Teacher 2020;58(5):330–4.
[28] Lázaro RPS, Fuentes-Aguilar RQ, Chairez I. Parametric characterization of approximation functions for the axial and lateral force between electromagnets and spherical permanent magnets. Measurement 2022.
[29] Bird JO, Chivers PJ. Electromagnetism and magnetic circuits. In: Newnes engineering and physical science pocket book. Elsevier; 1993, p. 77–87.
[30] Driver RD. Methods of A. M. Lyapunov and their application. SIAM Rev Soc Ind Appl Math 1965;7(4):570–1.
[31] Raj SA, Muthukumaran E, Jayakrishna K. A case study of 3D printed PLA and its mechanical properties. Mater Today Proc 2018;5(5, Part 2):11219–26.
[32] Farah S, Anderson DG, Langer R. Physical and mechanical properties of PLA, and their functions in widespread applications — A comprehensive review. Adv Drug Deliv Rev 2016;107:367–92.
[33] Bogue R. 3D printing: The dawn of a new era in manufacturing? Assem Autom 2013;33.